

Geophysical Research Letters

RESEARCH LETTER

10.1029/2020GL090042

Special Section:

Atmospheric Rivers:
Intersection of Weather and
Climate

Key Points:

- Atmospheric rivers (ARs) can be characterized as moisture or wind dominated (“wet” or “windy”)
- For a given level of vapor transport, “windy” ARs generally produce greater precipitation than do “wet” ARs
- Pacific Northwest ARs are becoming increasingly moisture dominated

Supporting Information:

- Supporting Information S1

Correspondence to:

K. R. Gonzales,
kgonzal@stanford.edu

Citation:





Gonzales, K. R., Swain, D. L., Barnes, E. A., & Diffenbaugh, N. S. (2020). Moisture- versus wind-dominated flavors of atmospheric rivers. *Geophysical Research Letters*, 47, e2020GL090042. <https://doi.org/10.1029/2020GL090042>

Received 29 JUL 2020

Accepted 12 NOV 2020

Accepted article online 20 NOV 2020

Moisture- Versus Wind-Dominated Flavors of Atmospheric Rivers

Katerina R. Gonzales¹ , Daniel L. Swain^{2,3,4} , Elizabeth A. Barnes⁵ ,
and Noah S. Diffenbaugh^{1,6} 

¹Department of Earth System Science, Stanford University, Stanford, CA, USA, ²Institute of the Environment and Sustainability, University of California, Los Angeles, CA, USA, ³The Nature Conservancy of California, San Francisco, CA, USA, ⁴Capacity Center for Climate and Weather Extremes, National Center for Atmospheric Research, Boulder, CO, USA, ⁵Department of Atmospheric Science, Colorado State University, Fort Collins, CO, USA, ⁶Woods Institute for the Environment, Stanford University, Stanford, CA, USA

Abstract Atmospheric rivers (ARs) are essential features of the global water cycle. Although AR definitions are commonly based on integrated vapor transport (IVT), ARs of a given IVT can induce a wide range of surface precipitation and wind impacts. We develop an AR “flavor” metric that partitions AR IVT into moisture-dominant and wind-dominant components. We use this metric to create a climatological catalog of “wet” and “windy” ARs along the U.S. West Coast from 1980 to 2016. Windy ARs are generally associated with stronger surface winds than are wet ARs, with the largest differences at low IVT. Windy ARs are also associated with greater daily precipitation totals than are wet ARs, with the difference widening at higher IVT, notably over mountainous regions. Pacific Northwest ARs have become increasingly moisture dominated over 1980–2016, which has important implications for western U.S. water availability and flood risk.

Plain Language Summary Atmospheric rivers transport large amounts of water vapor and are often associated with heavy precipitation and strong winds. Just as terrestrial rivers have different types, we show that the water vapor transport in atmospheric rivers can have distinct “flavors” and may be dominated by either high levels of moisture or strong winds. We find that atmospheric rivers of differing flavors produce different precipitation amounts and wind speeds. We also find that Pacific Northwest atmospheric rivers have become increasingly moisture dominated over the past four decades.

1. Introduction

In the western United States and beyond, atmospheric rivers (ARs) have earned a reputation for leading to both beneficial and harmful outcomes depending on their intensity (Dettinger, 2013; Dettinger et al., 2011; Ralph et al., 2019). These narrow filamentary corridors of water vapor transport can yield extreme precipitation and high surface winds, especially when associated with a strong low-level jet and orographic enhancement (Ralph et al., 2005). Most ARs deliver beneficial precipitation that serves to boost scarce Western water resources (Dettinger et al., 2011; Guan et al., 2010), but the strongest ARs often induce hazards such as floods and debris flows (Oakley et al., 2018) and damaging surface winds (Waliser & Guan, 2017).

Well-defined corridors of integrated vapor transport (IVT) are an important feature of ARs (Rutz et al., 2019). AR precipitation is positively correlated with IVT (Rutz et al., 2014), and AR storm total precipitation increases with AR duration (Lamjiri et al., 2017). The recently developed AR-CAT severity index, which is based on IVT and duration (Ralph et al., 2019), has been shown to strongly correlate with storm damages (Corringham et al., 2019). Various other characteristics also contribute to AR impacts, including geometry (Espinoza et al., 2018; Rutz et al., 2019), moisture source (Dacre et al., 2015; Kim et al., 2017; Nusbaumer & Noone, 2018; Sodemann & Stohl, 2013), genesis-to-landfall track (Gonzales et al., 2019; Guan & Waliser, 2019; Zhou & Kim, 2019), and temperature (Gonzales et al., 2019). Recent work, especially since the Atmospheric River Tracking Intercomparison Project (ARTMIP) (Shields et al., 2018), has laid a foundation for systematic descriptions of various AR characteristics detected by a suite of algorithms.

Compared to precipitation, surface wind impacts have received relatively little attention in the AR literature. Strong AR surface winds can damage trees and infrastructure, resulting in economic damages (Huang,

Swain, & Hall, 2020; Waliser & Guan, 2017). In their global evaluation, Waliser and Guan (2017) showed that ARs are associated with wind extremes in many regions.

Although IVT and the IVT-based AR-CAT index represent a critical first step in informing stakeholders of possible storm impacts, the wide diversity of AR characteristics suggests that there may be additional aspects of AR transport that are important for precipitation and/or surface winds. Previous case studies point to extreme ARs with various large-scale and mesoscale characteristics, including moist ARs that produce very little precipitation (Papineau & Holloway, 2012), moist and windy ARs that produce copious precipitation (e.g., Pineapple-Express-type ARs; Shields & Kiehl, 2016), ARs that are extremely warm and moist (Luo et al., 2015), and ARs with embedded mesoscale convective features (Cannon et al., 2018; Luo et al., 2015; Moore et al., 2012).

These studies highlight the need to further distinguish important aspects of individual AR events that may not be reflected by IVT, for both managing present-day risks and understanding future climate change. We thus investigate three questions: (1) What is the climatology of moisture- vs. wind-dominated AR flavors? (2) Are there differences in precipitation and surface winds associated with these flavors? (3) Has AR moisture dominance changed over the past several decades?

2. Methods & Data

2.1. Data

We use the 1980–2016 AR catalog from the AR detection algorithm first described in Mundhenk, Barnes, and Maloney (2016) and revised in Ralph et al. (2018), to select ARs that make landfall along the U.S. West Coast from October to May. We use the MERRA-2 reanalysis (Gelaro et al., 2017) to characterize ARs and the associated state of the atmosphere; the Parameter-elevation Regressions on Independent Slopes Model (PRISM) product (Daly et al., 2008) to characterize precipitation; and the Automated Surface Observing System (ASOS; automated airport surface weather station observations) 2-min sustained wind directions and speeds to characterize surface winds. See supporting information for additional details.

2.2. Moisture Dominance Metric and Flavor Characterization

We partition IVT into wind-varying IVT with moisture held constant at mean values ($IVTu'v'$), and moisture-varying IVT with wind held constant at mean values ($IVTq'$). At each grid box and pressure level, we calculate \bar{u} , \bar{v} , and \bar{q} by taking the calendar-day mean from 1980 to 2016 and applying a 60-day running mean. Full field IVT is shown in Equation 1, after Lavers et al. (2012). $IVTu'v'$ and $IVTq'$ are derived similarly, but instead using \bar{u} , \bar{v} , and \bar{q} associated with each grid box, pressure level, and calendar day (Equations 2 and 3):

$$IVT = \sqrt{\left(\frac{1}{g} \int_{1,000 \text{ hPa}}^{500 \text{ hPa}} qu \, dp\right)^2 + \left(\frac{1}{g} \int_{1,000 \text{ hPa}}^{500 \text{ hPa}} qv \, dp\right)^2} \quad (1)$$

$$IVTq' = \sqrt{\left(\frac{1}{g} \int_{1,000 \text{ hPa}}^{500 \text{ hPa}} q\bar{u} \, dp\right)^2 + \left(\frac{1}{g} \int_{1,000 \text{ hPa}}^{500 \text{ hPa}} q\bar{v} \, dp\right)^2} \quad (2)$$

$$IVTu'v' = \sqrt{\left(\frac{1}{g} \int_{1,000 \text{ hPa}}^{500 \text{ hPa}} \bar{q}u \, dp\right)^2 + \left(\frac{1}{g} \int_{1,000 \text{ hPa}}^{500 \text{ hPa}} \bar{q}v \, dp\right)^2} \quad (3)$$

Beginning with all AR timestamps in the catalog, we screen out non-landfalling AR objects across the North Pacific and conduct our analysis on each respective landfalling AR object. For every AR object, we take the average of $IVTu'v'$ and $IVTq'$ within the AR mask. We then standardize the populations of daily-mean AR $IVTu'v'$ and $IVTq'$ values by their z-scores (Figure 1). We define “moisture dominance” as the distance from the neutral one-to-one line (Figure 1a). To characterize the ARs into flavors, we bin them into tertiles along

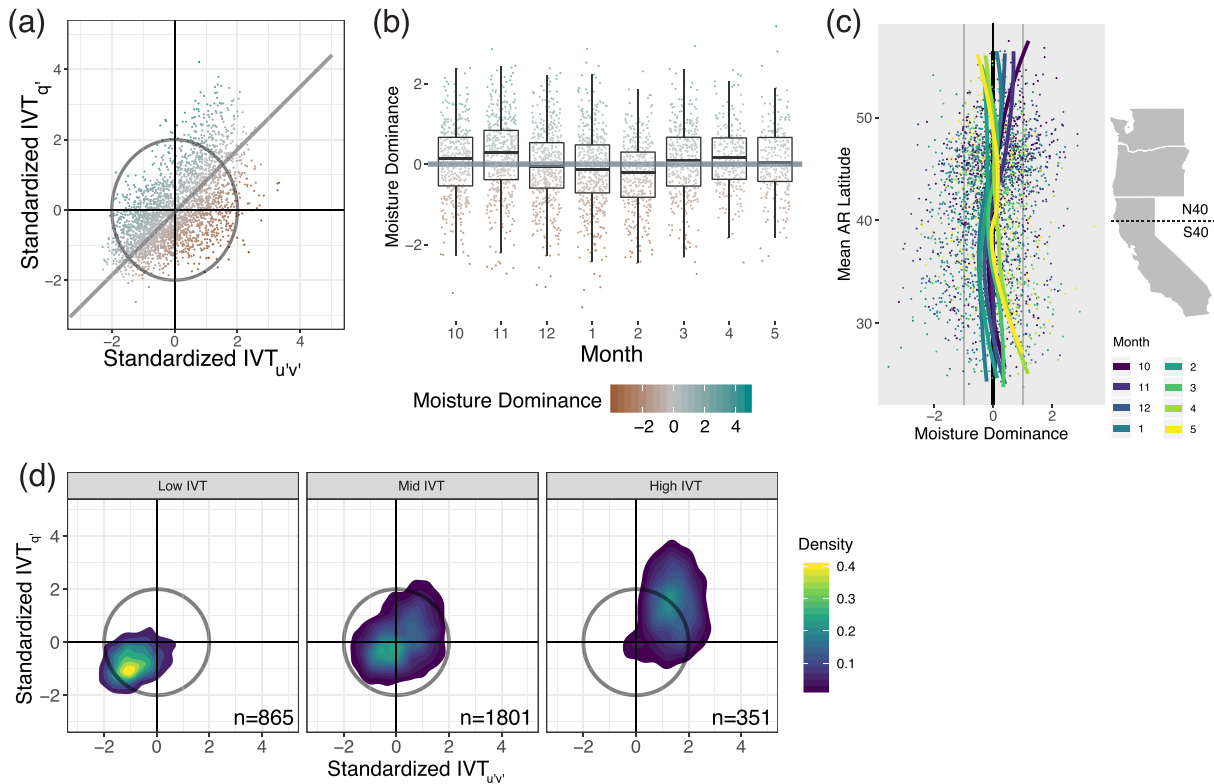


Figure 1. (a) The 1980–2016 climatology of extended cool season (October–May) AR days in moisture-wind space, defined by $IVTq'$ and $IVTu'v'$ and colored by “moisture dominance,” which is defined as distance from the neutral one-to-one line. (b) AR moisture dominance distributions by month, with the neutral line for reference. (c) AR moisture dominance values by latitude and colored by month. Curves are loess regressions at every latitude for each month and show variations in average moisture dominance between the months. (d) Density of AR days in moisture-wind space, colored by daily-mean IVT value and binned into three IVT ranges: low (300 kg/m/s and below), middle (300 to 500 kg/m/s), and high (500 kg/m/s and above).

the moisture dominance axis: The third of events with high moisture dominance are characterized as moisture dominant (the “wet” flavor), and the third of events with low moisture dominance are characterized as wind dominant (the “windy” flavor).

3. Results and Discussion

3.1. Climatology of AR Moisture Dominance

We characterize the flavor of each landfalling U.S. West Coast AR that occurred during October–May of 1980–2016 (Figure 1a). Although average AR moisture dominance exhibits some seasonal variation, the range of moisture dominance values varies widely within months (Figure 1b). (Monthly distributions of $IVTq'$, $IVTu'v'$, and IVT are shown in supporting information Figure S1.) AR moisture dominance likewise exhibits substantial variation within latitudinal bands (Figure 1c), suggesting that moisture dominance is not primarily regulated by latitude. The monthly-mean moisture dominance curves do shift toward higher values south of 30°N in April and May and north of 45°N in October and November.

The distribution of ARs in moisture-wind space varies substantially by IVT level (Figure 1d). Low- and mid-IVT ARs both exhibit relatively symmetric distributions, with both standardized $IVTq'$ and $IVTu'v'$ values falling within ± 2 standard deviations of the origin. In contrast, the distribution of high-IVT ARs spans a much wider range of standardized $IVTq'$ values (approaching 4 standard deviations) than standardized $IVTu'v'$ values, suggesting greater variability of moisture dominance than wind dominance across the strongest ARs.

3.2. Surface Winds and Precipitation by AR Flavor

A key question for assessing the importance of the AR flavor framework is whether the identified flavors manifest in distinct surface conditions, such as winds and precipitation. Station-average daily maximum

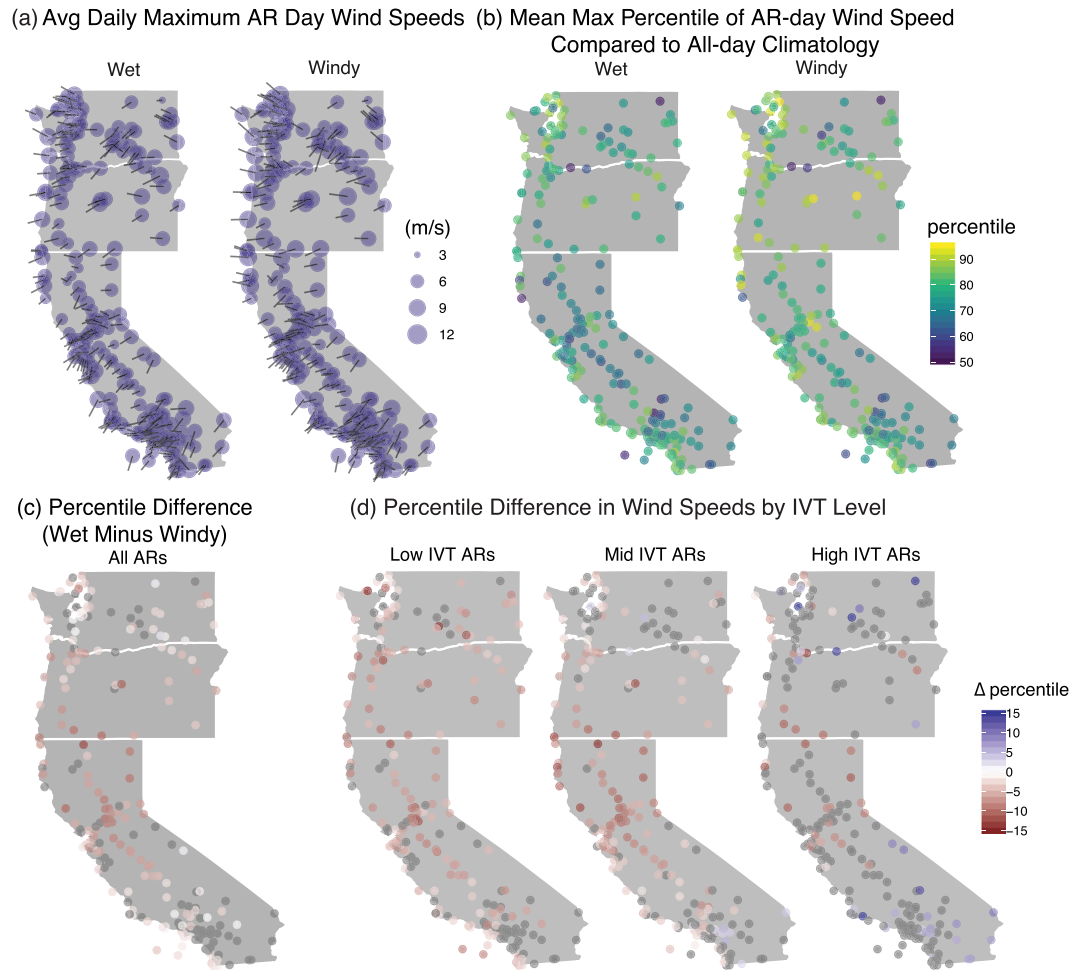


Figure 2. (a) Composite daily maximum station wind speeds and direction by AR flavor. Wind speeds are 2-min sustained speeds from ASOS. (b) Composite percentile ranking of AR daily maximum wind speeds by flavor, compared with the distribution of all-day climatological wind speeds at each station. Note that the p50 or higher rankings are expected due to the AR detection criteria for IVT, which is 250 kg/m/s higher than climatology. (c) Difference in station-average maximum wind speed rankings, wet minus windy (red denotes higher ranking for windy ARs). (d) Differences as in (c) but by IVT level. Stations with insignificant ($p > 0.05$) differences are in gray, determined by a two-sided Mann-Whitney U test.

2-min sustained wind speeds reach up to 12 m/s in both AR flavors (Figure 2a). Generally, coastal stations exhibit stronger winds than do inland stations during AR days, but this is not ubiquitous, as stations in mountainous areas also exhibit high wind speeds. Figure 2a demonstrates a latitudinal gradient in mean wind direction during AR days: from northwesterly around 48°N, to westerly in northern California and Oregon, to southwesterly in central California, to south-southwesterly in southern California. ARs of either flavor produce wind speeds ranking high in the all-day climatology (Figure 2b). As might be expected, windy ARs generally result in more extreme surface winds than do wet ARs (Figures 2c and 2d), particularly during low- and mid-IVT ARs (Figure 2d). However, during high-IVT ARs, relatively few stations exhibit statistically significant differences in wind speed between flavors (Figure 2d), and some southern California stations show wet ARs ranking significantly higher. Overall, stations generally exhibit higher wind rankings during windy ARs than during wet ARs, especially in low-IVT events.

Wet ARs and windy ARs produce statistically significant differences in precipitation (Figure 3), with windy ARs generally producing higher magnitudes, particularly over complex topography. We investigate AR-associated precipitation separately for northern and southern ARs (hereafter “N40” and “S40”, respectively, based on whether the AR object centroid location was north or south of 40°N; see section S2). As IVT increases, windy ARs generally produce successively greater magnitudes of precipitation than do wet

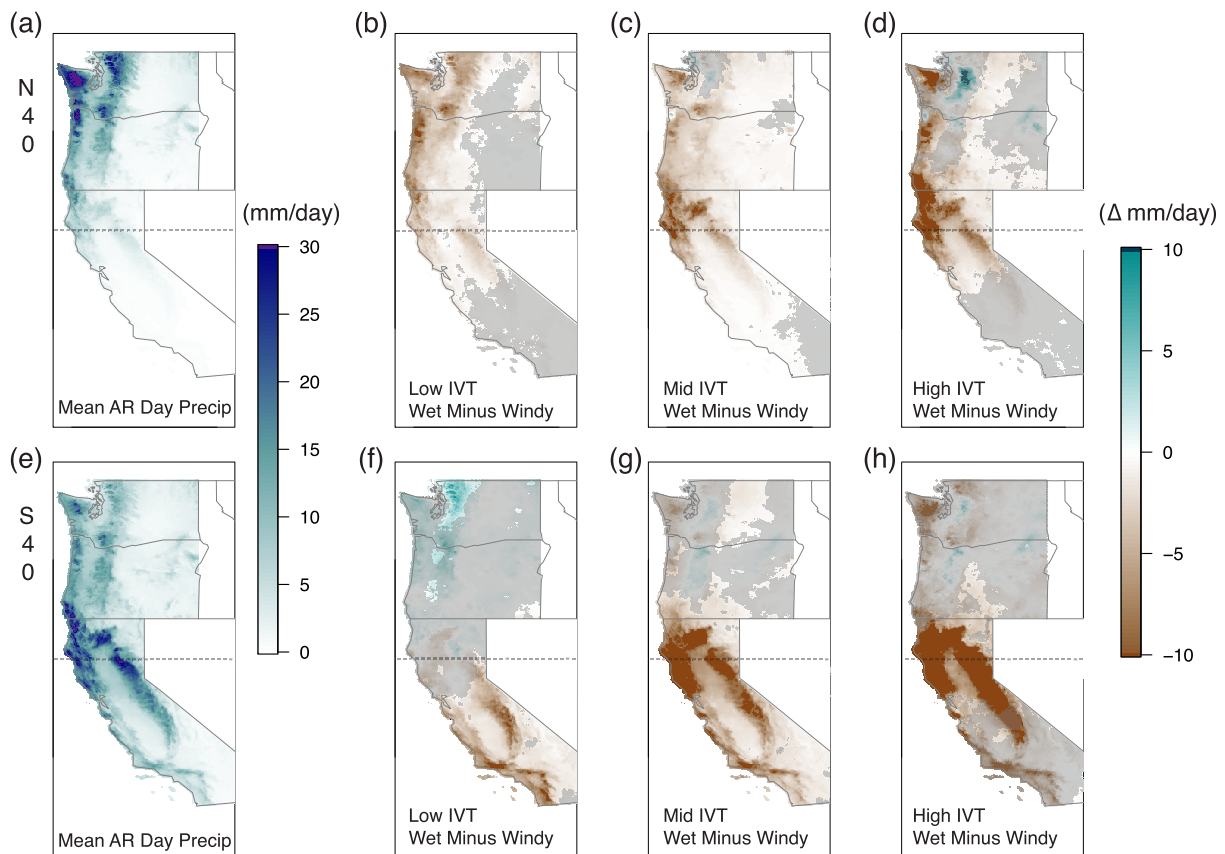


Figure 3. (a) Precipitation composite for N40 ARs. (b–d) N40 composite precipitation differences between flavors by IVT range bins (low, middle, and high as in Figure 1). Cool colors denote wet AR precipitation greater than windy AR precipitation. All regions without a gray overlay denote statistically significantly different precipitation distributions ($p < 0.05$) between flavors by a two-sided Mann-Whitney U test. (e–h) As in (a)–(d), but for S40 ARs. Due to the availability of the PRISM precipitation data, precipitation composites include ARs that occurred from 1981 to 2016 (see supporting information).

ARs over the landfall region (Figure 3). These differences are significant ($p < 0.05$; Figure S2) across most of the landfall region in both N40 and S40 composites and are particularly conspicuous in mountainous areas, which show large (> 10 mm/day) precipitation anomalies in the high-IVT bin (e.g., over the Sierra Nevada in the S40 composite and the Cascades in the N40 composites; Figure 3). The broadest exception to this pattern is the area of statistically significant positive precipitation anomalies over the Cascades in Washington and Oregon in the low-IVT S40 composite—far afield from the AR centroid latitude. Note that events classified as S40 do not preclude precipitation in northern half of domain due to the occurrence of meridionally extensive ARs (e.g., Figure 1c in Mundhenk, Barnes, & Maloney, 2016); however, it is currently unclear which processes would cause wet ARs to be associated with more precipitation than windy ARs in far-afield locations. Overall, these results suggest that AR flavor—particularly wind dominance—strongly modulates precipitation magnitudes, with the differences between flavors generally increasing over orography and at higher IVT.

3.3. Environmental Characteristics Associated With AR Flavors

Analyses of IVT composites and AR object axes reveal differences in average AR position and orientation between flavors (Figures 4a–4d). S40 ARs appear *on average* to make landfall with a westerly orientation, compared to a southwesterly orientation for N40 ARs. (Note that orientation differences between AR flavors are relative to the composite AR orientation in the landfalling region.) Windy ARs make landfall with an approximately southwesterly orientation to the coast (Figures 4b and 4d), while wet ARs make landfall with an approximately westerly (or even northwesterly) orientation (Figures 4a and 4c). The northwesterly orientation in the composite AR axis is most pronounced for S40 (i.e., southern California) wet ARs (Figure 4d).

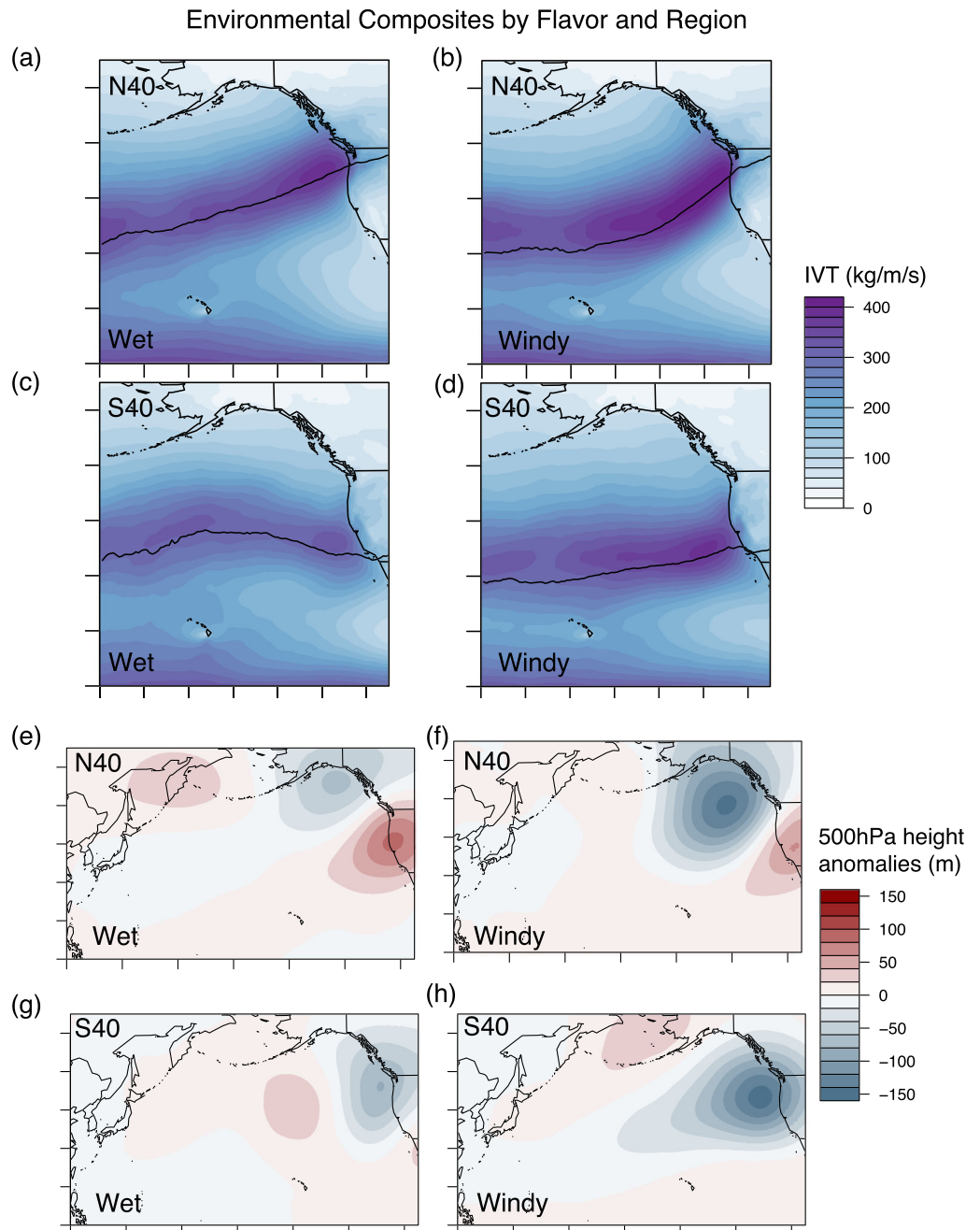


Figure 4. (a) Composite IVT and AR axis for wet N40 ARs. Composite median AR axes in (a)–(d) are calculated using all landfalling AR objects of this flavor. (b) Composite IVT and AR axis for windy N40 ARs. (c) Composite IVT and AR axis for wet S40 ARs. (d) Composite IVT for windy S40 ARs. (e–h) Composites as in (a)–(d) but composite 500-hPa geopotential height anomalies.

The differences in IVT composites are reflected in 500-hPa geopotential height anomalies (Figures 4e–4h). In both regions, windy ARs are associated with substantially lower than average heights over the Gulf of Alaska and northeast Pacific, suggestive of a deepened Aleutian Low. For wet N40 ARs (Figure 4e), geopotential height composites exhibit positive anomalies over California and modestly negative anomalies over the Gulf of Alaska. For wet S40 ARs (Figure 4g), geopotential height composites exhibit negative anomalies off the coast and positive anomalies over the central Pacific—suggestive of upstream blocking and the potential for downstream Rossby wave breaking, which has been previously identified as an important

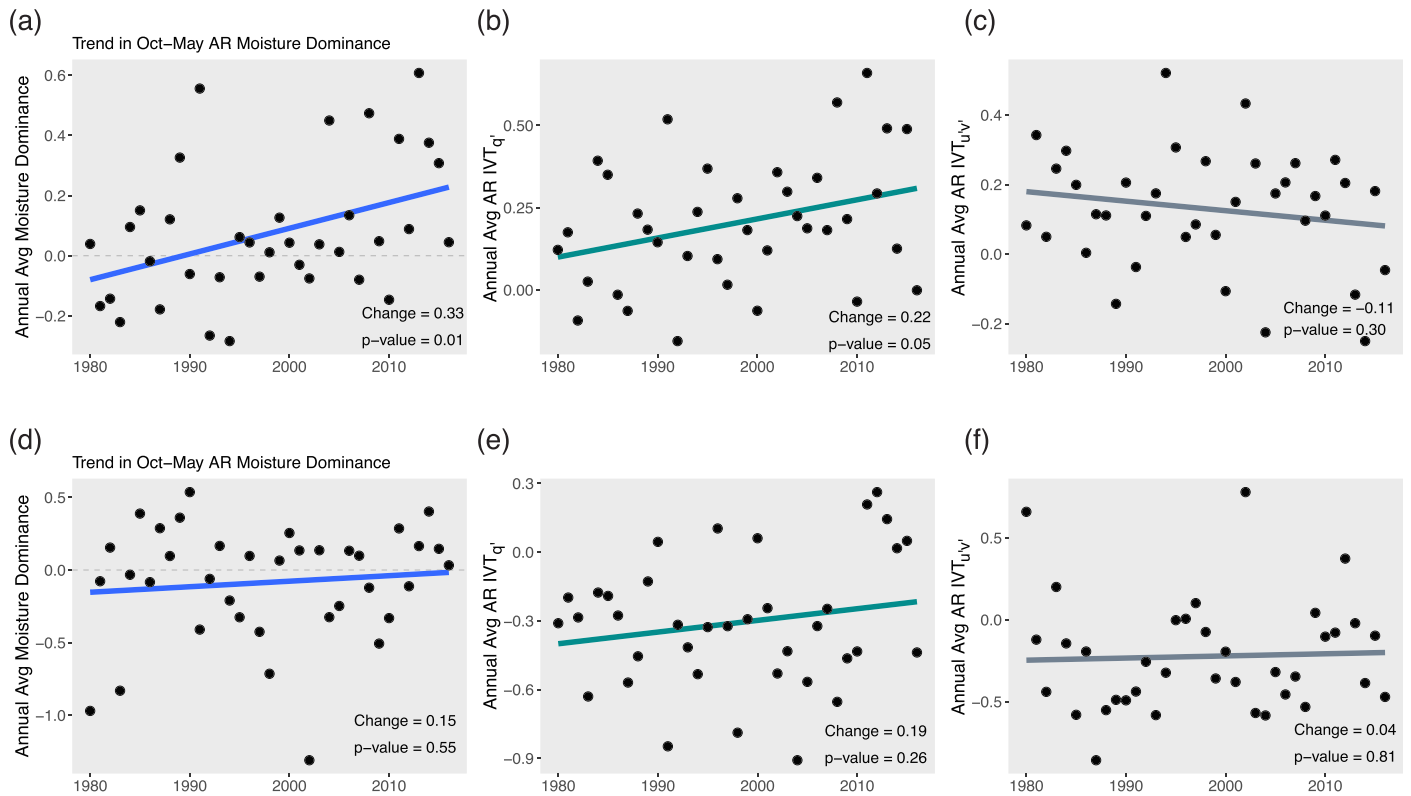


Figure 5. N40 AR trends in calendar-year-average quantities: (a) moisture dominance, (b) IVT_q', (c) IVT_{u'v'}'. (d–f) Same as (a)–(c) but for S40 ARs. Change over the 37-year period is noted in each panel, as well as p-values evaluated from *F*-tests.

AR-generating mechanism (Benedict et al., 2019). These IVT and geopotential height anomaly composite differences between flavors are most apparent in the mid- and high-IVT levels for both regions (Figures S3 and S4). Thus, although there are no statistically significant differences in composite location-relative AR tracks between AR flavors (Figure S5), the environmental composites reveal that some differences between wet and windy flavors are related to large-scale conditions over the North Pacific and their influence on AR position at landfall (Figure 4).

The contrasting composite IVT and height patterns (Figure 4) are consistent with literature describing large-scale characteristics associated with AR precipitation. Hecht and Cordeira (2017) described two AR clusters with differing orientations—westerly (or zonal) and southwesterly (or more meridional), with the southwesterly cluster associated with higher precipitation over northern California. Furthermore, Hu et al. (2017) found that West Coast ARs associated with cyclonic (vs. anticyclonic) Rossby wave breaking have different orientations and regionally dependent orographically induced precipitation impacts: ARs associated with anticyclonic wave breaking are characterized by relatively zonal orientation at landfall, while ARs associated with cyclonic wave breaking are more meridional (southwesterly). A hypothesis for future investigation is thus that moisture dominance is linked to Rossby wave breaking type; i.e., that cyclonic breaking is associated with windy ARs, and anticyclonic breaking with wet ARs. More generally, the fact that Rossby wave breaking is frequently associated with ARs (86% of occurrences) along the U.S. West Coast (Mundhenk, Barnes, Maloney, & Nardi, 2016) suggests that Rossby wave breaking is an important dynamical mechanism to focus on in future analyses of AR moisture dominance.

3.4. Changes in Moisture Dominance

We find that AR moisture dominance has significantly ($p = 0.01$) increased in the N40 region over 1980–2016 (Figure 5a). This N40 moisture dominance trend arises from both a strong and statistically significant positive trend in IVT_q' ($p = 0.05$) and a slight negative trend in IVT_{u'v'}' ($p = 0.30$) (Figures 5b and 5c). S40 ARs exhibit no trend in moisture dominance (Figure 5d), but a slight positive trend in IVT_q' ($p = 0.26$), with little indication of change in IVT_{u'v'}' (Figures 5e and 5f). Note that the sample size is substantially larger for N40 AR days

(1,846) than S40 AR days (1,171), likely contributing to the relative strength of the N40 signal. While we detect no statistically significant increase in S40 AR moisture dominance during 1980–2016, moisture dominance may increase in the future as the climate continues to warm and AR sample size increases—which strongly motivates analysis of the latest generation of coordinated global climate model simulations.

By definition, an increase in moisture dominance may arise from an increase in $IVTq'$, a decrease in $IVTu'v'$, or a combination of both. We find that both factors are present in the northern region. These opposing trends in N40 $IVTu'v'$ and $IVTq'$ motivate analysis of the underlying physical causes of trends in the individual constituent drivers of AR moisture dominance, including the relative roles of global warming and natural variability.

A positive trend in $IVTq'$ (Figures 5b and 5e) is consistent with the hypothesis that the moisture component of AR moisture transport increases with warming (Payne et al., 2020, and references therein) due to relatively straightforward thermodynamic processes. Indeed, West Coast ARs have already warmed by as much as 2°C since 1980 (Gonzales et al., 2019), strengthening the hypothesis that increasing N40 $IVTq'$ may be a signature of long-term climate change. However, we do not detect a significant increase in S40 $IVTq'$, even though AR warming has occurred in California. This discrepancy suggests that although the influence of atmospheric warming on moisture dominance may be emerging, it is not yet detectable for all regions over the study period. Application of a formal detection and attribution (D&A) framework will be necessary to more definitively quantify the influence of historical global warming on AR moisture dominance.

Interestingly, although other studies have shown an observed increase in AR IVT due to thermodynamic influences (e.g., Gershunov et al., 2019), our analyses do not indicate an increase in landfalling AR IVT over 1980–2016 (Figure S6). This may be due to the competing influences of decreasing wind velocity and increasing atmospheric moisture over the same period, particularly in the Pacific Northwest, which may be acting to temporarily mask or reduce the magnitude of any positive trend in IVT due to climate change. However, even if the distribution of AR IVT were to remain the same, differential moisture dominance trends by IVT level (Figure S7) could have implications for future changes in AR precipitation (Figure 3). A combination of shifting IVT distributions (Payne et al., 2020), changes in AR frequency (e.g., Espinoza et al., 2018; Gao et al., 2015), possible decreases in the orographic precipitation efficiency (i.e., the precipitation-to-IVT ratio; Huang, Swain, Walton, et al., 2020), and increases in AR moisture dominance (Figure 5a) may suggest even more substantial changes to surface impacts in the future.

4. Conclusions

We develop a new framework that characterizes AR “flavors” on a spectrum between “wet” (moisture-dominated IVT) and “windy” (wind-dominated IVT). We quantify the climatology of landfalling U.S. West Coast AR flavors from 1980 to 2016 and find an increase in AR moisture dominance over the Pacific Northwest during that period.

The distinction between wet and windy AR flavors can be consequential for surface impacts. Windy ARs are generally associated with higher wind speeds, particularly at low- and mid-IVT levels. Likewise, windy ARs are associated with larger precipitation accumulations—an effect that generally strengthens at higher IVT levels, particularly over mountainous regions (likely due to the role of wind forcing in orographic enhancement). The two AR flavors are associated with distinct large-scale environmental patterns. Most notably, there is a stronger mid-atmospheric low pressure anomaly adjacent to the landfall region for windy events compared to the composite geopotential height pattern during wet events. We find no statistically distinct difference in typical pre-landfall AR pathways between flavors, but we do find that the orientation of the composite IVT axis is more southwesterly for windy ARs than for wet ARs at landfall.

This study highlights the complexity of AR characteristics and motivates targeted regional disambiguation of ARs by moisture dominance in order to better predict surface impacts. We suggest that the emerging trend in northern U.S. West Coast moisture dominance may plausibly be a signature of climate change but requires verification using formal “D&A” analysis. Irrespective of the underlying cause, however, the observed moisture dominance trend suggests that changes in AR characteristics may arise even in the absence of overall IVT trends. Given the important role of moisture dominance in shaping AR precipitation outcomes (Figure 3), these findings may have substantial implications for present and future western U.S. water resources and flood management.

Our results motivate further research toward understanding the thermodynamic and kinematic characteristics of wet and windy AR flavors. Key topics for further investigation include (1) local and/or remote processes that influence the moisture or wind dominance of individual ARs; (2) the predictability of AR moisture dominance from synoptic to seasonal scales; and (3) future changes to AR flavors—and associated surface winds and precipitation—in response to continued global warming. These applications of the moisture dominance framework may help predict, project, and prepare for the potential hazards induced by ARs in present and future climates.

Data Availability Statement

The MERRA-2 reanalysis was downloaded online (<https://doi.org/10.5067/QBZ6MG944HW0>). The AR detection algorithm as originally written in Mundhenk, Barnes, and Maloney (2016) is available online (<http://hdl.handle.net/10217/170619>). The PRISM data are available at the PRISM Climate Group site (<https://prism.oregonstate.edu/historical/>), and the ASOS data are available at an online archive (<https://mesonet.agron.iastate.edu/request/download.phtml>).

Acknowledgments

We thank two anonymous reviewers for constructive and insightful comments and suggestions. Support for this work comes, in part, from NSF fellowship DGE-114747 (K. R. G.), Stanford University (K. R. G. and N. S. D.), DOE (N. S. D.), and NOAA grant NA19OAR4590151 (E. A. B.). D. L. S. was supported by a joint collaboration between the Institute of the Environment and Sustainability at the University of California, Los Angeles; the Center for Climate and Weather Extremes at the National Center for Atmospheric Research; and the Nature Conservancy of California.

References

- Benedict, J. J., Clement, A. C., & Medeiros, B. (2019). Atmospheric blocking and other large-scale precursor patterns of land falling atmospheric rivers in the North Pacific: A CESM2 study. *Journal of Geophysical Research: Atmospheres*, *124*, 11,330–11,353. <https://doi.org/10.1029/2019JD030790>
- Cannon, F., Hecht, C. W., Cordeira, J. M., & Ralph, F. M. (2018). Synoptic and mesoscale forcing of Southern California extreme precipitation. *Journal of Geophysical Research: Atmospheres*, *123*, 13,714–13,730. <https://doi.org/10.1029/2018JD029045>
- Corringham, T. W., Ralph, F. M., Gershunov, A., Cayan, D. R., & Talbot, C. A. (2019). Atmospheric rivers drive flood damages in the western United States. *Science Advances*, *5*, eaax4631. <https://doi.org/10.1126/sciadv.aax4631>
- Dacre, H. F., Clark, P. A., Martinez-Alvarado, O., Stringer, M. A., & Lavers, D. A. (2015). How do atmospheric rivers form? *Bulletin of the American Meteorological Society*, *96*, 1243–1255. <https://doi.org/10.1175/BAMS-D-14-00031.1>
- Daly, C., Halbleib, M., Smith, J. I., Gibson, W. P., Doggett, M. K., Taylor, G. H., et al. (2008). Physiographically sensitive mapping of climatological temperature and precipitation across the conterminous United States. *International Journal of Climatology*, *28*(15), 2031–2064. <https://doi.org/10.1002/joc.1688>
- Dettinger, M. D. (2013). Atmospheric rivers as drought busters on the U.S. West Coast. *Journal of Hydrometeorology*, *14*, 1721–1732. <https://doi.org/10.1175/JHM-D-13-02.1>
- Dettinger, M. D., Ralph, F. M., Das, T., Neiman, P. J., & Cayan, D. R. (2011). Atmospheric rivers, floods and the water resources of California. *Watermark*, *3*(2), 445–478. <https://doi.org/10.3390/w3020445>
- Espinoza, V., Waliser, D. E., Guan, B., Lavers, D. A., & Ralph, F. M. (2018). Global analysis of climate change projection effects on atmospheric rivers. *Geophysical Research Letters*, *45*, 4299–4308. <https://doi.org/10.1029/2017GL076968>
- Gao, Y., Lu, J., Leung, L. R., Yang, Q., Hagos, S., & Qian, Y. (2015). Dynamical and thermodynamical modulations on future changes of landfalling atmospheric rivers over western North America. *Geophysical Research Letters*, *42*, 7179–7186. <https://doi.org/10.1002/2015GL065435>. Received
- Gelaro, R., McCarty, W., Suárez, M. J., Todling, R., Molod, A., Takacs, L., et al. (2017). The Modern-Era Retrospective Analysis for Research and Applications, version 2 (MERRA-2). *Journal of Climate*, *30*, 5419–5454. <https://doi.org/10.1175/JCLI-D-16-0758.1>
- Gershunov, A., Shulgina, T., Clemesha, R. E. S., Guirguis, K., Pierce, D. W., Dettinger, M. D., et al. (2019). Precipitation regime change in western North America: The role of atmospheric Rivers. *Scientific Reports*, *9*, 9944. <https://doi.org/10.1038/s41598-019-46169-w>
- Gonzales, K. R., Swain, D. L., Nardi, K. M., Barnes, E. A., & Diffenbaugh, N. S. (2019). Recent warming of landfalling atmospheric rivers along the West Coast of the United States. *Journal of Geophysical Research: Atmospheres*, *124*, 2018JD029860. <https://doi.org/10.1029/2018JD029860>
- Guan, B., Molotch, N. P., Waliser, D. E., Fetzer, E. J., & Neiman, P. J. (2010). Extreme snowfall events linked to atmospheric rivers and surface air temperature via satellite measurements. *Geophysical Research Letters*, *37*, L20401. <https://doi.org/10.1029/2010GL044696>
- Guan, B., & Waliser, D. E. (2019). Tracking atmospheric rivers globally: Spatial distributions and temporal evolution of life cycle characteristics. *Journal of Geophysical Research: Atmospheres*, *124*, 12,523–12,552. <https://doi.org/10.1029/2019JD031205>
- Hecht, C. W., & Cordeira, J. M. (2017). Characterizing the influence of atmospheric river orientation and intensity on precipitation distributions over North Coastal California. *Geophysical Research Letters*, *44*, 9048–9058. <https://doi.org/10.1002/2017GL074179>
- Hu, H., Dominguez, F., Wang, Z., Lavers, D. A., Zhang, G., & Ralph, F. M. (2017). Linking Atmospheric river hydrological impacts on the U. S. West Coast to Rossby wave breaking. *Journal of Climate*, *30*, 3381–3399. <https://doi.org/10.1175/JCLI-D-16-0386.1>
- Huang, X., Swain, D. L., & Hall, A. D. (2020). Future precipitation increase from very high resolution ensemble downscaling of extreme atmospheric river storms in California. *Science Advances*, *6*, eaba1323. <https://doi.org/10.1126/sciadv.aba1323>
- Huang, X., Swain, D. L., Walton, D. B., Stevenson, S., & Hall, A. D. (2020). Simulating and evaluating atmospheric river-induced precipitation extremes along the U.S. Pacific Coast: Case studies from 1980–2017. *Journal of Geophysical Research: Atmospheres*, *125*, e2019JD031554. <https://doi.org/10.1029/2019JD031554>
- Kim, H.-M., Zhou, Y., & Alexander, M. A. (2017). Changes in atmospheric rivers and moisture transport over the Northeast Pacific and western North America in response to ENSO diversity. *Climate Dynamics*, *52*, 7375–7388. <https://doi.org/10.1007/s00382-017-3598-9>
- Lamjiri, M. A., Dettinger, M. D., Ralph, F. M., & Guan, B. (2017). Hourly storm characteristics along the U.S. West Coast: Role of atmospheric rivers in extreme precipitation. *Geophysical Research Letters*, *44*, 7020–7028. <https://doi.org/10.1002/2017GL074193>
- Lavers, D. A., Villarini, G., Allan, R. P., Wood, E. F., & Wade, A. J. (2012). The detection of atmospheric rivers in atmospheric reanalyses and their links to British winter floods and the large-scale climatic circulation. *Journal of Geophysical Research*, *117*, D20106. <https://doi.org/10.1029/2012JD018027>

- Luo, Q., Tung, W., Luo, Q., & Tung, W. (2015). Case study of moisture and heat budgets within atmospheric rivers. *Monthly Weather Review*, *143*, 4145–4162. <https://doi.org/10.1175/MWR-D-15-0006.1>
- Moore, B. J., Neiman, P. J., Ralph, F. M., & Barthold, F. E. (2012). Physical processes associated with heavy flooding rainfall in Nashville, Tennessee, and vicinity during 1–2 May 2010: The role of an atmospheric river and mesoscale convective systems. *Monthly Weather Review*, *140*(2), 358–378. <https://doi.org/10.1175/MWR-D-11-00126.1>
- Mundhenk, B. D., Barnes, E. A., & Maloney, E. D. (2016). All-season climatology and variability of atmospheric river frequencies over the North Pacific. *Journal of Climate*, *29*, 4885–4903. <https://doi.org/10.1175/JCLI-D-15-0655.1>
- Mundhenk, B. D., Barnes, E. A., Maloney, E. D., & Nardi, K. M. (2016). Modulation of atmospheric rivers near Alaska and the U.S. West Coast by northeast Pacific height anomalies. *Journal of Geophysical Research: Atmospheres*, *121*, 12,751–12,765. <https://doi.org/10.1002/2016JD025350>
- Nusbaumer, J., & Noone, D. (2018). Numerical evaluation of the modern and future origins of atmospheric river moisture over the West Coast of the United States. *Journal of Geophysical Research: Atmospheres*, *123*, 6423–6442. <https://doi.org/10.1029/2017JD028081>
- Oakley, N. S., Lancaster, J. T., Hatchett, B. J., Stock, J., Ralph, F. M., Roj, S., & Lukashov, S. (2018). A 22-year climatology of cool season hourly precipitation thresholds conducive to shallow landslides in California. *Earth Interactions*, *22*, 1–35. <https://doi.org/10.1175/EI-D-17-0029.1>
- Papineau, J., & Holloway, E. (2012). The dry side of atmospheric rivers in Alaska, Anchorage Forecast Office Research Papers, NOAA/NWS/ARH. [Available online at <http://citeseerx.ist.psu.edu/viewdoc/summary?doi=10.1.1.729.4947>.]
- Payne, A. E., Demory, M.-E., Leung, L. R., Ramos, A. M., Shields, C. A., Rutz, J. J., et al. (2020). Responses and impacts of atmospheric rivers to climate change. *Nature Reviews Earth & Environment*, *1*, 143–157. <https://doi.org/10.1038/s43017-020-0030-5>
- Ralph, F. M., Neiman, P. J., Rotunno, R., Ralph, F. M., Neiman, P. J., & Rotunno, R. (2005). Dropsonde observations in low-level jets over the northeastern Pacific Ocean from CALJET-1998 and PACJET-2001: Mean vertical-profile and atmospheric-river characteristics. *Monthly Weather Review*, *133*(4), 889–910. <https://doi.org/10.1175/MWR2896.1>
- Ralph, F. M., Rutz, J. J., Cordeira, J. M., Dettinger, M., Anderson, M., Reynolds, D., et al. (2019). A scale to characterize the strength and impacts of atmospheric rivers. *Bulletin of the American Meteorological Society*, *100*, 269–289. <https://doi.org/10.1175/BAMS-D-18-0023.1>
- Ralph, F. M., Wilson, A. M., Shulgina, T., Kawzenuk, B., Sellars, S., Rutz, J. J., et al. (2018). ARTMIP—Early start comparison of atmospheric river detection tools: How many atmospheric rivers hit northern California's Russian River watershed? *Climate Dynamics*, *52*, 4973–4994. <https://doi.org/10.1007/s00382-018-4427-5>
- Rutz, J. J., Shields, C. A., Lora, J. M., Payne, A. E., Guan, B., Ullrich, P., et al. (2019). The Atmospheric River Tracking Method Intercomparison Project (ARTMIP): Quantifying uncertainties in atmospheric river climatology. *Journal of Geophysical Research: Atmospheres*, *124*, 13,777–13,802. <https://doi.org/10.1029/2019JD030936>
- Rutz, J. J., Steenburgh, W. J., & Ralph, F. M. (2014). Climatological characteristics of atmospheric rivers and their inland penetration over the western United States. *Monthly Weather Review*, *142*, 905–921. <https://doi.org/10.1175/MWR-D-13-00168.1>
- Shields, C. A., & Kiehl, J. T. (2016). Simulating the Pineapple Express in the half degree Community Climate System Model, CCSM4. *Geophysical Research Letters*, *43*, 7767–7773. <https://doi.org/10.1002/2016GL069476>
- Shields, C. A., Rutz, J. J., Leung, L.-Y., Ralph, F. M., Wehner, M., Kawzenuk, B., et al. (2018). Atmospheric River Tracking Method Intercomparison Project (ARTMIP): Project goals and experimental design. *Geoscientific Model Development*, *11*, 2455–2474. <https://doi.org/10.5194/gmd-11-2455-2018>
- Sodemann, H., & Stohl, A. (2013). Moisture origin and meridional transport in atmospheric rivers and their association with multiple cyclones. *Monthly Weather Review*, *141*, 2850–2868. <https://doi.org/10.1175/MWR-D-12-00256.1>
- Waliser, D., & Guan, B. (2017). Extreme winds and precipitation during landfall of atmospheric rivers. *Nature Geoscience*, *10*, 179–183. <https://doi.org/10.1038/ngeo2894>
- Zhou, Y., & Kim, H. (2019). Impact of distinct origin locations on the life cycles of landfalling atmospheric rivers over the U.S. West Coast. *Journal of Geophysical Research: Atmospheres*, *124*, 11,897–11,909. <https://doi.org/10.1029/2019JD031218>